

Non-nesting spin-density-wave antiferromagnetism in FeAs from first principles

David Parker

Oak Ridge National Laboratory, 1 Bethel Valley Road, Oak Ridge, Tennessee 37831, USA

I. I. Mazin

U.S. Naval Research Laboratory, 4555 Overlook Avenue SW, Washington, D.C. 20375, USA

(Received 15 February 2011; revised manuscript received 17 March 2011; published 2 May 2011)

The antiferromagnetic (AFM) state of FeAs is very different from that of the FeAs-based superconductor parent compounds, and it is rather complicated, with the Fe spins forming an incommensurate magnetic spiral pattern with a wavelength of about 15 Å. To model this, we perform first-principles calculations and find the nearest-neighbor AFM ordering to be energetically favorable, with the lowest-energy pattern reproducing the experimentally found nearest-neighbor correlations. Other AFM orderings are also very stable, although higher in energy. Unlike in the superconductor parent compounds, the Fermi-surface geometry thus plays a small role. We calculate the bare Lindhard susceptibility in the AFM state and find that the observed spin-density-wave ordering vector $\mathbf{Q} \simeq (0,0,0.4)$ is *not* that given by this calculation. This is again unlike the superconductor parent compounds, which generally show a magnetic pattern matching the Lindhard susceptibility maximum. Thus in FeAs, the observed pattern must be due to a subtler mechanism.

DOI: [10.1103/PhysRevB.83.180403](https://doi.org/10.1103/PhysRevB.83.180403)

PACS number(s): 75.40.Gb, 71.20.Gj, 74.70.Xa

In February 2008, the Hosono group¹ discovered superconductivity with a comparatively high T_c of 26 K in fluorine-doped LaFeAsO. A frenzy of experimental and theoretical activity then ensued, with additional families being identified, including the “122” compounds $A\text{Fe}_2\text{As}_2$ ($A = \text{Ba}, \text{Ca}, \text{Sr}, \text{and Eu}$), the “111” materials such as LiFeAs, the “11” materials FeTe and FeSe, and still others. A maximum T_c of 55 K, second only to that observed in the cuprates, was observed fairly early on² in the Sm-doped 1111 compound. The common factor in all these materials is that superconductivity occurs near a parent compound (usually based on FeAs, with the exception of the chalcogenides) exhibiting a spin-density-wave (SDW) state. Major issues under study currently include the symmetry of the superconducting state and the nature of the parent compound magnetism, in particular a combination of local and itinerant behavior. The interested reader is referred to review articles³ for more detailed information.

Despite this flurry of activity surrounding the iron arsenide superconductors, much less work has been done on the simple binary FeAs. Unlike the generally tetragonal (or nearly so) structure of the FeAs-based superconductors, FeAs has a highly orthorhombic structure (space group 62, $Pnma$, $a = 3.384$ Å, $b = 5.475$ Å, $c = 6.063$ Å) with three distinct distances comprising the six Fe-Fe nearest neighbors, and the nearly ideal Fe-As tetrahedra so prominent in the superconductor parent compounds are notably absent. Given these differences, it is perhaps not surprising that the experimental properties of FeAs are rather different from those of the superconductor parent compounds; as described in Refs. 4 and 5, FeAs orders antiferromagnetically at a T_{AFM} of approximately 70 K, and the ordering is a noncollinear spiral, with an *incommensurate* ordering vector of approximately $(0,0,0.38$ to $0.40)$.^{4,6} This is in marked contrast with the commensurate ordering observed in the superconductor parent compounds. Like the FeAs-based compounds, this material is metallic, but the easily evident similarities end there. Notably, the experimentally detected relatively long-period (one period involves 20 Fe atoms) incommensurate spiral does not develop

on a background of a ferromagnetic (FM) ordering, when the relative angle between the nearest-neighbor spins is small, but on an antiferromagnetic (AFM) background, where four nearest neighbors form angles close to 180° , and two close to 0° .

In this paper, we present first-principles calculations of this unusual compound, focusing specifically on the magnetism in this material. We find as the lowest energy magnetic pattern allowed within the four formula unit cell an AFM ordering, consistent with the background antiferromagnetism found experimentally, so that the four nearest neighbors (at 2.81 and 2.95 Å) have opposite spins and the next two (at 3.38 Å) have parallel ones. Note that the Fe-As-Fe bond angle for the latter pair is close to 90° (87.99°), while for the former four the angles are much flatter (69.93° and 75.37° , respectively) so the above pattern is consistent with the Goodenough-Kanamori rules.⁷ These, of course, had been derived for dielectrics and are not necessarily applicable to itinerant metals, but this coincidence suggests that some local physics is present. An analogy with Fe-based superconductors⁸ suggests that the magnetic moments on Fe are formed by the local Hund’s rule coupling (which, unlike the Hubbard U , is not screened out in metals), while the lowest energy pattern is defined by all occupied states and not just the states near the Fermi level. This is supported by the analysis of another calculated AFM structure, as discussed below.

The first possible explanation for this unusual magnetism that comes to mind is that of an initially *commensurate* antiferromagnetic state, such as the AF2 state described below, which may form for strong-coupling reasons such as superexchange or others. In this scenario, this state would then provide the background upon which an SDW would develop “accidentally,” as a result of Fermi surface geometry that happened to be favorable, i.e., “nesting” or “nesting-like,” as suggested in Ref. 9.

However, even before performing any calculations, one finds problems with this hypothesis. In particular, another compound containing the basic FeAs unit⁹ shows nearly the

TABLE I. Magnetic ordering energies (per Fe) of various states.

| State | Ordering energies | |
|-------|---------------------|--|
| | ΔE (meV/Fe) | |
| PM | 0 | |
| FM | -50 | |
| AF1 | -82 | |
| AF2 | -100 | |

same ordering wave vector and ordering temperature, which would require that both materials “accidentally” have the same Fermi surface geometry. For instance, the “nesting” suggestion of Ref. 9 is based on a visual analysis of the calculated Fermi surface in the *nonmagnetic state*, even though the SDW develops on a background of a commensurate AFM state with a very large ($M > 2\mu_B/\text{Fe}$) magnetic moment. Since the nesting concept is only valid in the linear perturbation regime over the state where the Fermi surface was calculated (nonmagnetic here), it is obviously inapplicable for such a strongly magnetic state. Besides, even in the linear response regime, the quantity controlling the SDW wave vector is the *real* part of the susceptibility, $\text{Re}\chi_0(\mathbf{q})$, and not the imaginary part that can possibly be related to visual “nesting.”¹⁰

With these thoughts in mind, we have performed first-principles calculations and evaluated the Lindhard bare spin susceptibility in the antiferromagnetic ground state of FeAs, the simplest of the FeAs-based compounds demonstrating incommensurate SDW's, and the least correlated of all ($M \sim 0.5\mu_B$), to check whether indeed a maximum in $\text{Re}\chi_0(\mathbf{q})$ appears at the right wave vector. After computing $\text{Re}\chi_0(\mathbf{q})$, we found *no correspondence whatsoever* between the observed ordering vector and maxima in $\text{Re}\chi_0(\mathbf{q})$. This means quite clearly that the reason for the observed ordering pattern must be sought elsewhere, perhaps involving frustration among the various possible magnetic states forming the background of the observed spiral ordering.

For the theoretical calculations, we have employed the generalized gradient approximation (GGA) of Perdew *et al.*,¹¹

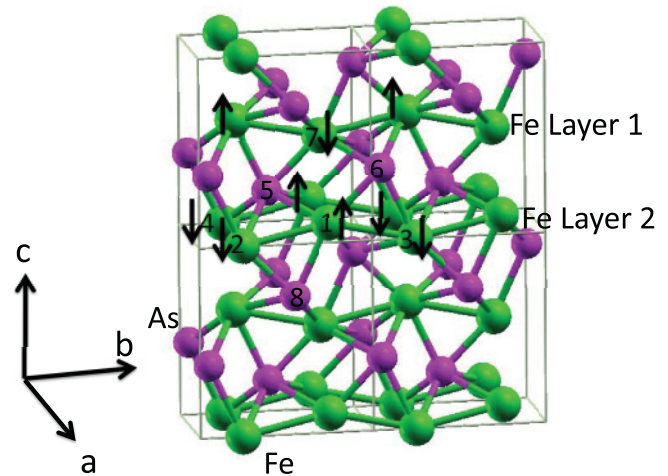


FIG. 1. (Color online) The chemical and magnetic structure of FeAs. Note that Fe sits inside a nearly perfect octahedron, but is substantially displaced toward one of the corners. Fe-Fe nearest-neighbor distances: 1-2 and 1-3, 2.806 Å; next-nearest, 1-7, 2.95 Å; next-next-nearest, 2-4, 3.384 Å. Fe-As bond angles: 1-8-2, 69.9°; 1-6-7, 75.4°. For the AF1 structure, the spins in Fe layer 1 are reversed.

as implemented in the code WIEN2K,¹² using approximately 1000 k points in the full Brillouin zone. No internal coordinate optimization was performed. Instead, we used the experimental structure as reported in Ref. 6.

FeAs presents a manifold of potential ordered states even within the same four-formula unit cell. Listed in Table I, in units of meV/Fe atom, are the ordering energies, relative to the paramagnetic state, of an FM state, as well as each of two possible AFM states, AF1 and AF2. In AF1, the nearest Fe neighbors (2.81 Å apart, see Fig. 1) are aligned ferromagnetically while the second neighbors (2.95 Å apart) are aligned antiferromagnetically, while in AF2 both nearest and next-nearest neighbors are aligned antiferromagnetically. For all states, the third Fe neighbors (3.384 Å) are aligned ferromagnetically. As indicated in the table, AF2 has a significantly lower energy than the other ordered states, and we note

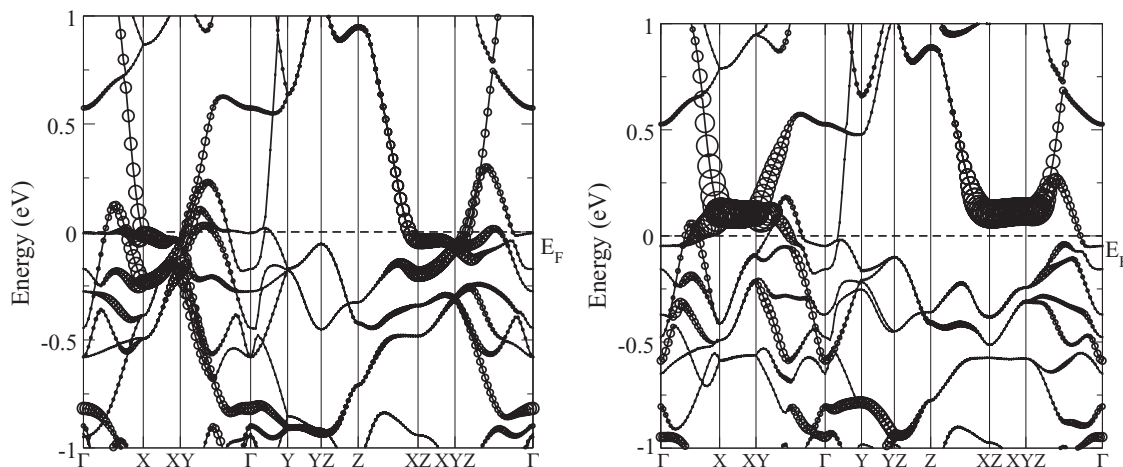


FIG. 2. The calculated band structures of FeAs in the paramagnetic state (left) and in the AF2 state (right), with Fe- $d_{3x^2-r^2}$ character indicated by the width of the circles. Note the disappearance of the flat PM band at E_F in the AF2 state, which has predominantly this character.

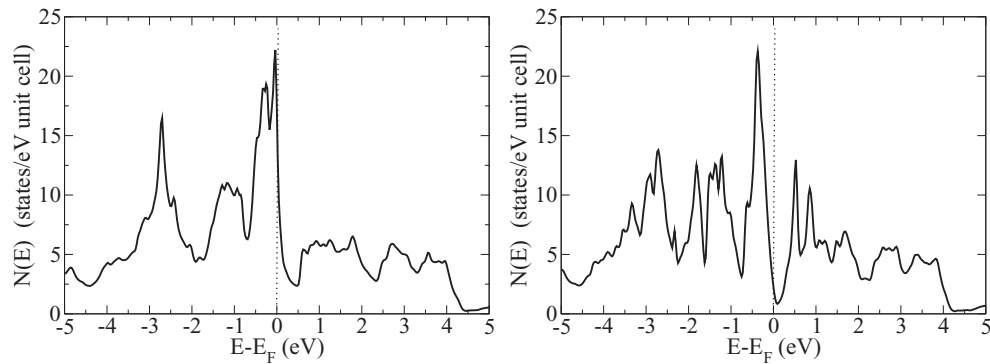


FIG. 3. The calculated densities of states of FeAs in the paramagnetic state (left) and in the AF2 state (right). Note the appearance of the pseudogap around E_F in the latter plot.

that, as described previously, the observed magnetic pattern is that of AF2. Assuming that this energetics is mappable onto the nearest-neighbor Ising model, we find $J_{2,81} = 4$ meV and $J_{2,95} = 9$ meV. While the signs are consistent with the standard superexchange, such a large (and counterintuitive) distance dependence indicates a more complicated picture. Indeed, we find that both AFM patterns create comparable pseudogaps at the Fermi level, and the additional gain for AF2 comes from deeper electronic states. Besides, the calculated bands do not show any distinct crystal field gap between the t_{2g} and e_g states, as expected for a quasi-octahedral coordination, but rather five strongly overlapping d bands. The ordered moment of this state is calculated as approximately $1.36\mu_B$ per Fe (1.2 in the LDA), which is significantly larger than the value of $0.5\mu_B$ obtained in the experiment. This is also a hallmark of itinerant magnetism: fluctuations beyond the mean-field level reduce the tendency to magnetism. However, we believe that the low-energy electronic structure obtained in the GGA is correct, or, if it errs, it errs in the opposite direction, toward smaller, not larger, residual Fermi surfaces, as is the case in BaFe_2As_2 and similar compounds.

In Figs. 2, 3, and 4, we present calculated results for the band structures, densities of states, and Fermi surfaces of FeAs within the paramagnetic (PM) and AF2 states, respectively. As expected, the antiferromagnetism substantially reconstructs the band structure so that the AF Fermi surface hardly

resembles that of the paramagnetic state. In particular, the high density of states (DOS) of the paramagnetic state, as indicated by the flat band at the Fermi level covering much of the paramagnetic band plot, as well as the rather extensive Fermi surfaces, are replaced by a pseudogapped phase that, while still metallic, has no such high DOS at E_F , and fewer band crossings and smaller Fermi surfaces as well. The only features from the PM state that are still extant in the AF2 state are the Γ -centered hole pockets, and the general Fe $d_{3x^2-r^2}$ character of the relevant bands. We mention in passing that, as in the superconducting materials, since the crystal field splitting is much smaller than the bandwidth, it is not visible on the band plots or the DOS. In addition, from inspecting the band and densities-of-states plots, one notes significant band-structure changes even a full eV from the Fermi level, so that the magnetism cannot be considered to be a Fermi surface nesting phenomenon; indeed, the rather complex PM Fermi surface of Fig. 4 does not exhibit obvious nesting tendencies, nor does the calculated $\text{Re}\chi_0$ show any relevant structure at the experimental wave vector.

We note that, similarly to the iron arsenide superconducting parent compounds, the Fermi surfaces in the AFM state are completely 3D, even though these are substantially anisotropic without the magnetism. Another similarity lies in the fact that the reconstructed Fermi surface is semimetallic, with an electron pocket at the Γ point and four hole pockets around

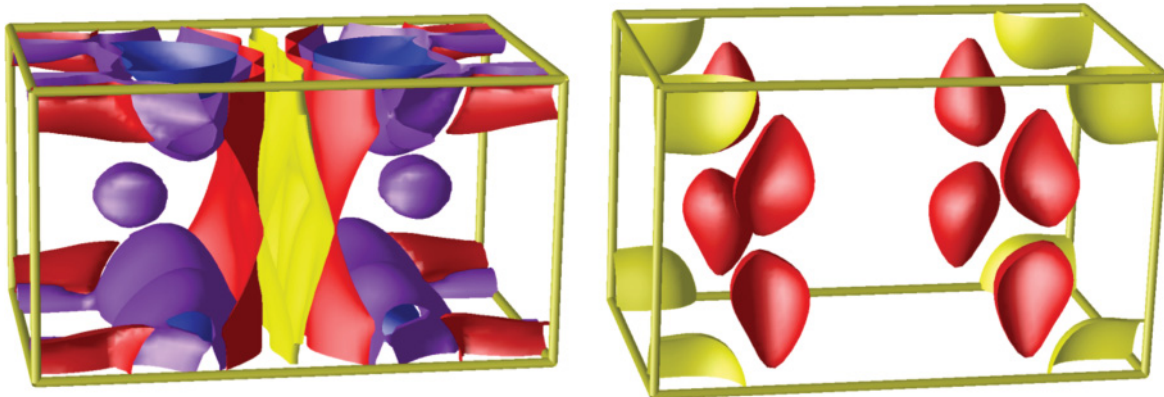


FIG. 4. (Color online) The calculated Fermi surfaces of FeAs in the paramagnetic (left) and in the AF2 state (right). For the AF2 state, the a axis is horizontal, the b axis vertical, and the c axis into the paper; for the paramagnetic state the b and c axes are reversed.

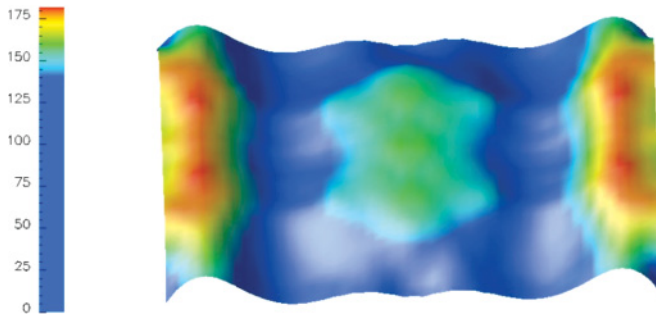


FIG. 5. (Color online) The real part of the Lindhard susceptibility (in arbitrary units) of FeAs in the bc plane in the AF1 state.

the $(\pm 0.25, \pm 0.3, 0)$ points. In Fig. 5, we show the calculated real part of the Lindhard spin susceptibility, which is given as follows:

$$\chi_0(\mathbf{q}) = \sum_{\alpha, \beta, \mathbf{k}} \frac{f(\epsilon_{\alpha, \mathbf{k}}) - f(\epsilon_{\beta, \mathbf{k}+\mathbf{q}})}{\epsilon_{\beta, \mathbf{k}+\mathbf{q}} - \epsilon_{\alpha, \mathbf{k}} + i\gamma}.$$

Here α and β are the band indices, \mathbf{k} and \mathbf{q} are wave vectors, and ϵ is the band energy. f is the Fermi function and the sum is taken over the Brillouin zone and over all relevant bands. We are using the constant matrix element approximation here. The Stoner¹³ criterion for an SDW instability is that at the SDW wave vector \mathbf{Q} , $\chi_0(\mathbf{Q})I(\mathbf{Q}) > 1$. If we neglect the momentum dependence of the vertex $I(\mathbf{q})$ (which can shift the position of the strongest instability off the maximum in χ_0 , but usually not by much), the instability occurs where χ_0 is large. In Fig. 5, we present a contour plot of the Lindhard susceptibility over the $x = 0$ plane (in this plot, the c axis is horizontal). The “ridge” of large values in fact traces out an arc beginning at approximately $(0, 0.25, 0)$ and contouring over vertically and then horizontally, reaching its absolute maximum at $\mathbf{Q} = (0, 0.34, 0.08)$ and the seven points related to this by symmetry.

We note that this theoretically calculated \mathbf{Q} differs substantially from the $(0, 0, 0.39)$ measured via neutron scattering.¹⁴

This tells us that the canonical picture⁹ of a nesting-driven SDW, either forming on the background of the nonmagnetic state or of an AF state, as in elemental Cr, *cannot be correct* for this system.

At this moment, it is hard to ascertain what the microscopic reason of the SDW modulation of the AFM state may be, except that it is not Fermi surface nesting. Complex long-range magnetic interactions, typical for itinerant but not weakly coupled magnetic systems, may create frustration that can in turn lead to incommensurability. This is particularly true in light of the small (18 meV) energy difference between the two lowest ordered states, and the possibility that still other ordered states, besides the two randomly selected configurations modeled here, exist. Our analysis does not prove frustration is active here, only that, unlike nesting, we cannot exclude it as the cause of the observed magnetic ordering. One can also recall that in parent compounds of Fe-based superconductors, for instance, biquadratic terms that potentially can lead to such frustration (even though in that case they do not) are anomalously large.

As an antecedent compound to the iron arsenide superconductors, FeAs is of considerable interest, with a rather distinct chemical structure as well as incommensurate spiral antiferromagnetic ordering. From our first-principles calculations, we find that this material appears to have a “two-stage” magnetism, similar to Cr metal, in which the experimentally observed order develops on top of an antiferromagnetic ordered state—the lowest energy state in the calculations. However, this order is *not* due to a nesting-type instability, for the order develops experimentally at a momentum far removed from that found in the calculations. It is likely that the correct description of this state involves, at the very least, a subtle interplay of interactions resulting from the manifold of potential ordered states.

This work was supported by the Office of Naval Research (I.I.M.) and by (D.P.) the U.S. Department of Energy, Basic Energy Sciences, Materials Sciences and Engineering.

¹Y. Kamihara, T. Watanabe, M. Hirano, and H. Hosono, *J. Am. Chem. Soc.* **130**, 3296 (2008).

²Z. A. Ren, W. Li, J. Wang, Y. Wei, X. L. Shen, Z. Cai, G. C. Che, X. L. Dong, L. L. Sun, F. Zhou, and Z. X. Zhao, *Chin. Phys. Lett.* **25**, 2215 (2008).

³P. C. W. Chu, A. Koshlev, W. Kwok, I. I. Mazin, U. Welp, and Hai-Hu Wen (editors), *Physica C* **469**, Issues 9–12 (2009). Special iron pnictide review.

⁴K. Selte, A. Kjekshus, and A. F. Andresen, *Acta. Chem. Scand.* **26**, 3101 (1973).

⁵K. Segawa and Y. Ando, *J. Phys. Soc. Jpn.* **78**, 104720 (2009).

⁶E. Rodriguez, C. Stock, K. Krycka, C. F. Majkrzak, K. Kirshenbaum, N. P. Butch, S. R. Shanta, J. Paglione, and M. Green, *Physical Review B* (to be published).

⁷J. B. Goodenough, *J. Phys. Chem. Solids* **6**, 287 (1958); J. Kanamori, *ibid.* **10**, 87 (1959).

⁸M. D. Johannes and I. I. Mazin, *Phys. Rev. B* **79**, 220510 (2009).

⁹Y. Nambu, L. L. Zhao, E. Morosan, K. Kim, G. Kotliar, P. Zajdel, M. A. Green, W. Ratcliff, J. A. Rodriguez-Rivera, and C. Broholm, *Phys. Rev. Lett.* **106**, 037201 (2011).

¹⁰M. D. Johannes, I. I. Mazin, and C. A. Howells, *Phys. Rev. B* **73**, 205102 (2006).

¹¹J. P. Perdew, K. Burke, and M. Ernzerhof, *Phys. Rev. Lett.* **77**, 3865 (1996).

¹²P. Blaha, K. Schwarz, G. K. H. Madsen, D. Kvasnicka, and J. Luitz, *WIEN2k, An Augmented Plane Wave + Local Orbitals Program for Calculating Crystal Properties* (Karlheinz Schwarz, Techn. Universität Wien, Austria, 2001).

¹³E. C. Stoner, *Philos. Mag. Ser. 7* **3**, 336 (1927).

¹⁴The real part of χ_0 calculated using the PM band structure (not shown) does not show any peak at the experimental wave vector either.